Radio Science, Volume 14, Number 6, pages 1135–1145, November–December 1979

A power law phase screen model for ionospheric scintillation 1. Weak scatter

C. L. Rino

SRI International, Menlo Park, California 94025

(Received January 18, 1979.)

In this paper the weak scatter scintillation theory is reformulated to show explicitly the ramifications of an arbitrarily large ionospheric outer scale. The measured temporal phase spectrum, for example, is effectively truncated at a fixed frequency corresponding to the detrend time or the length of the data interval over which it is measured (whichever is smaller). As a consequence, the rms phase exhibits a complicated dependence on the relative irregularity drift velocity and the propagation geometry. This effect has not been included in previous analyses. By comparison, intensity scintillation data are intrinsically high-pass filtered by the diffraction process. By taking advantage of this fact a simple closed form expression for the S_4 intensity scintillation index has been derived. The theory is applied to representative data sets from the Wideband satellite. The interpretation of the ionospheric parameters deduced from the analysis is also discussed.

1. INTRODUCTION

The scintillation of transionospheric radio waves is a subject of both scientific interest and practical concern. It is known that randomly irregular electron density variations along propagation paths cause a variety of scintillation effects. Moreover, it is now generally accepted that the size distribution of the 'irregularities' can be characterized by a power law spectral density function (SDF) [*Rufenach*, 1972; *Dyson et al.*, 1974; *Phelps and Sagalyn*, 1976; *Crane*, 1976; *McClure et al.*, 1977].

Only recently, however, have the ramifications of the fact that the power law continuum encompasses at least 3 orders of magnitude in scale size [*Yeh and Liu*, 1977; *Crane*, 1976] begun to be considered. The high-frequency cutoff or inner scale is controlled by diffusive processes. *Booker and Ferguson* [1978] have inferred an inner-scale cutoff near the ion gyroradius (~5 m).

The low-frequency cutoff or outer scale is presently not well understood. An outer-scale parameter may well be an intrinsic property of the instability that causes the irregularities. In practice, however, the effective outer scale emerges as a somewhat arbitrary division between the well-developed structures that can be modeled by a statistically homogeneous random process and the evolving structures that depend on the initial configuration of the plasma at the time of instability onset.

The available evidence shows that the ionospheric outer scale, if indeed a verifiable outer scale exists at all, is at least several tens of kilometers. Such dimensions are larger than the Fresnel radii at the lowest frequencies of interest (VHF) for typical ionospheric propagation geometries. Thus Fresnel filtering will remove any effects of the outer scale in intensity scintillation data.

By comparison, phase scintillation data respond directly to large-scale structures. Two situations can arise. It is usually assumed that the data interval is long when it is compared with the appropriate temporal period that corresponds to the outer scale. In that case the rms phase is well defined and proportional to the outer scale. More often, however, the opposite situation prevails, and the length of the data interval determines the magnitude of the rms phase.

In this paper the weak scatter theory is reformulated to show explicitly the ramifications for data interpretation of an arbitrarily large outer scale. Phase scintillation is treated in section 2, intensity scintillation is treated in section 3, and the results are applied to actual ionospheric data in section 4. Finally, in section 5 the relationship between in situ measurements and scintillation data is discussed in light of the reformulated theory.

The analysis is based on the phase-screen model that has been used since the early development

0048-6604/79/1112-1135$01.00

of the scintillation theory [*Booker et al.*, 1950; *Bramley*, 1954; *Ratcliffe*, 1956; *Mercier*, 1962; *Briggs and Parkin*, 1963; *Salpeter*, 1967; *Rufenach*, 1975]. The validity of this approach has recently been demonstrated by *Bramley* [1977], who showed that an equivalent phase screen accurately reproduces the amplitude and phase scintillation calculated by using the more complicated formulation that accommodates diffraction within the scattering region provided that the height of the phase screen is appropriately chosen.

As a practical matter, the phase-screen model provides a means of obtaining unique, equivalent lumped parameters that characterize the average irregularity structure along the propagation path. The ramifications of structure variations and geometrical smearing within the disturbed region must ultimately be determined by much more elaborate calculations.

2. PHASE SCINTILLATION

When both the measurement frequency f and the phase reference frequency f_r are well above the plasma frequency, the zeroth-order approximation to the differential phase $\delta\phi$ is given by the line integral

$$\delta\phi \cong -r_e\lambda \int \Delta N_e\, dl(1 - (f/f_r)^2) \tag{1}$$

where r_e is the classical electron radius, λ is the wave length, and ΔN_e is the local electron density perturbation. The integral is evaluated along the straight line path from the signal source to the receiver.

Let $\Phi_{\Delta N_e}(\vec{\kappa}, \kappa_z)$ represent the three-dimensional SDF of $\Delta N_e(\vec{r})$. If $f_r \gg f$, it is shown in the work of *Rino and Fremouw* [1977] that the phase SDF in a plane transverse to the z axis has the general form

$$\Phi_{\delta\phi}(\vec{\kappa}) = r_e^2\lambda^2 L \sec^2\theta \Phi_{\Delta N_e}(\vec{\kappa}, -\tan\theta\, \hat{a}_{k_T} \cdot \vec{\kappa}) \tag{2}$$

where L is the layer thickness, θ is the zenith angle, and $\hat{a}_{k_T}$ is a unit vector along the xy plane projection of the propagation vector $\vec{k}$. In this particular formulation of the problem the z axis is normal to the scattering layer. Thus the propagation angles enter explicitly.

The three-dimensional phase autocorrelation function (ACF) is derived from (2), which is formally two dimensional, by using the Fourier transform relation [*Rino and Fremouw*, 1977]:

$$R_{\delta\phi}(\Delta\vec{\rho}, \Delta z) = r_e^2\lambda^2 L \sec^2\theta \cdot \iint \Phi_{\Delta N_e}(\vec{\kappa}, -\tan\theta\, \hat{a}_{k_T} \cdot \vec{\kappa}) \cos(\vec{\kappa} \cdot \Delta\vec{\rho}_s) \frac{d\vec{\kappa}}{(2\pi)^2} \tag{3}$$

where

$$\Delta\vec{\rho}_s = \Delta\vec{\rho} - \tan\theta\, \hat{a}_{k_T} \Delta z \tag{4}$$

Thus the Δz dependence, which is important for data interpretation, is explicitly contained in the model.

To proceed, the functional form of $\Phi_{\Delta N_e}(\vec{\kappa}, \kappa_z)$ must be specified. In the work of *Rino and Fremouw* [1977] it is shown that for a fairly general anisotropy model, $\Phi_{\Delta N_e}$ in (2) can be written as

$$\Phi_{\Delta N_e}(\vec{\kappa}, -\tan\theta\, \hat{a}_{k_T} \cdot \vec{\kappa}) = ab\langle \Delta N_e^2 \rangle Q([A\kappa_x^2 + B\kappa_x\kappa_y + C\kappa_y^2]^{1/2}) \tag{5}$$

The parameters a and b are axial ratios along and transverse to the principal irregularity axis, respectively. The coefficients A, B, and C depend on the propagation angles relative to the principal irregularity axis (see (41) of *Rino and Fremouw*, [1977]).

The function $Q(q)$ gives the shape of the SDF. It is normalized to unit area. Thus for a power law SDF with no inner-scale cutoff, the appropriate functional form is

$$Q(q) = \frac{8\pi^{3/2}\Gamma(\nu + \frac{1}{2})/\Gamma(\nu - 1) q_0^{2\nu-2}}{[q_0^2 + q^2]^{\nu+1/2}} \tag{6}$$

where q_0 is the outer-scale cutoff wave number. Equation (6) can be derived from the more general form given in Table 2 of *Rino and Fremouw* [1977] by taking the limit as the inner scale approaches zero. By making the definition

$$C_s = 8\pi^{3/2}\langle \Delta N_e^2 \rangle q_0^{2\nu-2}\Gamma(\nu + \tfrac{1}{2})/\Gamma(\nu - 1) \tag{7}$$

it follows that $\Phi_{\Delta N_e}(q) = abC_s q^{-(2\nu+1)}$ for all wave numbers $\vec{\kappa}$ such that $q \gg q_0$. It is understood here that

$$q^2 = A\kappa_x^2 + B\kappa_x\kappa_y + C\kappa_y^2 \tag{8}$$

The parameter C_s, which has been called the strength of turbulence by *Rumsey* [1975], is closely related to the structure constant that is used in classical turbulence studies [*Strohbehn*, 1968]. The principal reason for introducing C_s (or the structure constant) is that, unlike $\langle \Delta N_e^2 \rangle$ or q_0, C_s can be unambiguously measured in an experiment. That is, if ΔN_e is sampled over an interval small in

comparison with $l_0 = 2\pi/q_0$, which is usually the case in practice, then neither q_0 nor $\langle \Delta N_e^2 \rangle$ can be uniquely determined. However, by using spectral analysis, C_s is uniquely calculable from a finite data segment.

By substituting (5) and (6) into (3) it can be shown with appropriate variable changes that

$$R_{\delta\phi}(y) = r_e^2 \lambda^2 L \sec\theta\, GC_s \int_0^\infty \frac{q J_0(qy)}{[q_0^2 + q^2]^{\nu+1/2}}\, dq/2\pi \tag{9}$$

where

$$G = \frac{ab}{\sqrt{AC - B^2/4\cos\theta}} \tag{10}$$

is a purely geometrical factor. To complete (9), y is replaced by $f(\Delta\vec{\rho}_s)$, where

$$f^2(\Delta\vec{\rho}_s) = \frac{C\Delta\rho_{s_x}^2 - B\Delta\rho_{s_x}\Delta\rho_{s_y} + A\Delta\rho_{s_y}^2}{AC - B^2/4} \tag{11}$$

A comparison of (8) and (11) will show that contours of constant phase correlation and contours of constant phase spectral density are mutually orthogonal ellipses, at least in terms of the complementary variables $\Delta\vec{\rho}_s$ and $\vec{\kappa}$. Recall, however, that $\Delta\vec{\rho}_s$ depends on Δz (see (4)).

The integral in (9) can be evaluated, giving the result

$$R_{\delta\phi}(y) = r_e^2 \lambda^2 L \sec\theta\, GC_s \left|\frac{y}{2q_0}\right|^{\nu-1/2} \frac{K_{\nu-1/2}(q_0 y)}{2\pi\,\Gamma(\nu + 1/2)} \tag{12}$$

where $K_\nu(x)$ is the modified Bessel function. In a typical experiment, only a temporal ACF is measured. The form of the temporal ACF can be derived from (12) by substituting $\vec{v}_T \delta t$ and $v_z \delta t$ into (11) for $\Delta\vec{\rho}$ and Δz, respectively, where $\vec{v} = (\vec{v}_T, v_z)$ is the relative velocity of the irregularities as seen by an observer in the reference coordinate system. Thus $\vec{v}$ includes a height-dependent component due to source motion as well as the true irregularity drift component.

The form of the temporal phase ACF can be compactly written as $R_{\delta\phi}(v_{\text{eff}}\delta t)$ where

$$v_{\text{eff}} = \left[\frac{Cv_{s_x}^2 - Bv_{s_x}v_{s_y} + Av_{s_y}^2}{AC - B^2/4}\right]^{1/2} \tag{13}$$

and

$$\vec{v}_s = \vec{v}_T - \tan\theta\, \hat{a}_{k_T} v_z \tag{14}$$

As was noted by *Rino and Fremouw* [1977], v_{eff} reduces to the component of $\vec{v}$ perpendicular to the line of sight, $v_\perp$, for isotropic irregularities. In general, $v_{\text{eff}} \leq v_\perp$, but in a highly anisotropic medium, v_{eff} can be much less than $v_\perp$ if the relative scan direction is along the principal irregularity axis.

The temporal power spectrum of phase is given by the Fourier integral

$$\varphi(f) = \int_{-\infty}^{\infty} R_{\delta\phi}(v_{\text{eff}}\delta t) \cos(2\pi i f \delta t)\, d\delta t \tag{15}$$

By using (12) for $R_{\delta\phi}(y)$, (15) can be evaluated, giving the result

$$\varphi(f) = \frac{T}{[f_0^2 + f^2]^{p/2}} \tag{16}$$

where

$$f_0 = v_{\text{eff}}\, q_0/2\pi = v_{\text{eff}}\, l_0 \tag{17}$$

$$p = 2\nu$$

and

$$T = r_e^2 \lambda^2 (L \sec\theta)\, GC_s \frac{\sqrt{\pi}\,\Gamma(\nu)}{(2\pi)^{2\nu+1}\,\Gamma(\nu + 1/2)}\, v_{\text{eff}}^{2\nu-1} \tag{18}$$

Equation (16) has the same form as (5) when (6) and (7) are used. Indeed, if $f \gg f_0$, $\varphi(f) = Tf^{-p}$. The phase power law index is 1 less than the power law index for the three-dimensional in situ SDF. Moreover, as will be discussed in section 4, the parameters T and p can be determined from differential phase measurements. Equation (18) relates the strength of turbulence C_s to the directly measurable parameter T. That is, it provides a basis for removing the purely geometrical dependence of the scattering.

To compute the phase variance, (16) is integrated over all frequencies, giving the result

$$\langle \delta\phi^2 \rangle = r_e^2 \lambda^2 (L \sec\theta)\, GC_s \frac{q_0^{-2\nu+1}\,\Gamma(\nu - 1/2)}{4\pi\,\Gamma(\nu + 1/2)} \tag{19}$$

which can also be obtained by evaluating the limiting form of (12) as y approaches zero. However, as was noted in section 1, if the data interval or the integration time τ_c (whichever is smaller) is less than f_0^{-1}, then the measured rms phase is not given by (19).

One means of allowing for this effect is to replace q_0 in (19) by $q_c = 2\pi/(v_{\text{eff}}\,\tau_c)$. This is equivalent to replacing f_0 in (16) by τ_c^{-1}. Alternatively, the expression

$$\langle \delta\phi^2 \rangle \cong 2T \int_{\tau_c^{-1}}^{\infty} f^{-p}\, df = \frac{2T}{p-1}\,\tau_c^{p-1} \tag{20}$$

can be used which gives a somewhat larger value for the rms phase than that given by (19) with q_0 replaced by q_c.

The important point to note here is that whenever $\tau_c < f_0^{-1}$, $\langle \delta\phi^2 \rangle$ cannot be uniquely defined because its value is dominated by the low-frequency portion of $\varphi(f)$. The precise shape of the low-frequency portion of a measured SDF is sensitive to the data processing procedure as well as small departures from strict homogeneity. Thus the rms phase is not a viable parameter for characterizing scintillation effects in a power law scattering medium as it is in a medium dominated by a single scale size.

Note also that when $\tau_c < f_0^{-1}$, $\langle \delta\phi^2 \rangle$ is proportional to $v_{\text{eff}}^{2\nu-1}$. Since v_{eff} varies strongly with altitude as well as changes in the propagation geometry, the behavior of $\langle \delta\phi^2 \rangle$ is considerably more complicated than it is in the usually assumed situation in which (19) is used with q_0 taken as a constant.

As a final comment, the measured differential phase is not strictly equivalent to $\delta\phi$ as given by (1), because diffraction effects change the phase structure. It will be shown in section 4, however, that the diffraction effects do not significantly change the interpretation of $\varphi(f)$ as described in this section, as long as the corresponding intensity scintillation is not too large.

3. INTENSITY SCINTILLATION

From the results developed of *Rino and Fremouw* [1977] it is easily shown that the intensity ACF corresponding to (3) is

$$R_{\delta I}(\Delta\vec{\rho}, \Delta z) = 4r_e^2\lambda^2\, L \sec^2\theta \int\int \Phi_{\Delta N_e}(\vec{\kappa}, -\tan\hat{a}_{k_T}\cdot\vec{\kappa}) \times \sin^2(h(\vec{\kappa})Z)\cos(\vec{\kappa}\cdot\Delta\vec{\rho}_s)\frac{d\kappa}{(2\pi)^2} \tag{21}$$

where

$$h(\vec{\kappa}) = \kappa^2 - \tan^2\theta(\hat{a}_{k_T}\cdot\vec{\kappa})^2 \tag{22}$$

and

$$Z = \frac{\lambda z_R \sec\theta}{4\pi} \tag{23}$$

In (23), $z_R = zz_s/(z + z_s)$, where z_s is the distance to the source. This modification of the plane wave results allows for wavefront curvature when the source distance is finite. The S_4 scintillation index is derived from the defining relation

$$S_4^2 = R_{\delta I}(0, 0) \tag{24}$$

Substituting (6), (7), and (8) into (21) and performing a series of variable changes gives

$$S_4^2 = 4r_e^2\lambda^2(L\sec\theta)\,ab \cdot \int\int \frac{C_s}{[q_0^2 + (A'q_x^2 + B'q_xq_y + C'q_y^2)]^{\nu+1/2}} \times \sin^2(q^2Z)\frac{d\vec{q}}{(2\pi)^2} \tag{25}$$

where

$$A' = [A\cos^2\varphi + B\sin\varphi\cos\varphi + C\sin^2\varphi]\cos^2\theta \tag{26a}$$

$$B' = [B\cos 2\varphi + (C - A)\sin 2\varphi]\cos\theta \tag{26b}$$

$$C' = [A\sin^2\varphi - B\sin\varphi\cos\varphi + C\cos^2\varphi] \tag{26c}$$

This manipulation puts the scintillation index formula in the Briggs-Parkin form which is most commonly used. The interrelationship is discussed by *Rino and Fremouw* [1977]. (Note that in the work of *Rino and Fremouw* [1977], (51*b*) is incorrect; (26*b*) is the correct form.)

As it stands, (25) cannot be evaluated analytically. *Rufenach* [1975] and *Costa and Kelley* [1976] have used a slightly modified form of (6) which can be evaluated when $\nu = 1.5$. However, in section 1 it was argued that for ionospheric scintillation $q_0^2 Z \ll 1$. In that case the constant portion of $[q_0^2 + (A'q_x^2 + B'q_xq_y + C'q_y^2)]^{-(\nu+0.5)}$ occurs where $\sin^2(q^2) \ll 1$. Thus it is a good approximation to take

$$S_4^2 = 4r_e^2\lambda^2(L\sec\theta)\,C_sZ^{\nu-1/2} \cdot \int\int \frac{ab\sin^2(q^2)\,dq/(2\pi)^2}{(A'q_x^2 + B'q_xq_y + C'q_y^2)^{\nu+1/2}} \tag{27}$$

which is the limiting form of (25) as $q_0 \to 0$.

Hereafter, the double integral in (27), which is now independent of Z, will be denoted by I.

To evaluate I, a coordinate rotation and variable separation is first performed, giving the intermediate result

$$I = \frac{1}{\pi^2} \int_0^\infty q^{-2\nu} \sin^2(q^2)\, dq \cdot \int_0^{\pi/2} \frac{ab\, d\phi}{[A'' - (A'' - C'')\sin^2\phi]^{\nu+1/2}} \tag{28}$$

where

$$A'' = \tfrac{1}{2}[A' + C' + D'] \tag{29a}$$

$$C'' = \tfrac{1}{2}[A' + C' - D'] \tag{29b}$$

and

$$D' = \sqrt{(A' - C')^2 + B'^2} \tag{29c}$$

Note that $A'' \geq C''$. The integral over q is well known from scattering by isotropic irregularities. It can be evaluated using *Gradshteyn and Ryzhik* [1965, formula 3.823]. A simpler form is

$$\int_0^\infty q^{-2\nu} \sin^2(q^2)\, dq = \frac{\sqrt{\pi}}{2} \frac{\Gamma((2.5 - \nu)/2)}{\Gamma((\nu + 0.5)/2)(\nu - 0.5)} \tag{30}$$

which is valid for ν values such that $0.5 < \nu < 2.5$.

Thus (27) can be simplified to

$$S_4^2 = r_e^2 \lambda^2 (L \sec\theta)\, C_s Z^{\nu-1/2} \cdot \left[\frac{\Gamma((2.5 - \nu)/2)}{2\sqrt{\pi}\,\Gamma((\nu + 0.5)/2)(\nu - 0.5)}\right] \mathscr{J} \tag{31}$$

where $\mathscr{J}$ is a combined geometry and propagation factor defined as

$$\mathscr{J} = \frac{2ab}{\pi A''^{(\nu+1/2)}} \int_0^{\pi/2} \frac{d\phi}{[1 - ((A'' - C'')/A'')\sin^2\phi]^{\nu+1/2}} \tag{32}$$

The integral in (32) can be evaluated in terms of the hypergeometric function ${}_2F_1(\alpha, \beta; \nu; z)$ [see *Gradshteyn and Ryzhik*, 1965, formula 3.681]. To avoid convergence problems when $A'' \gg C''$, however, the transformation

$${}_2F_1(\alpha, \beta; \nu; z) = (1 - z)^{\nu - \alpha - \beta}\, {}_2F_1(\nu - \alpha, \nu - \beta; \nu; z) \tag{33}$$

can be used. The final result is

$$\mathscr{J} = \frac{ab}{\sqrt{A''}\, C''^{\nu}}\, {}_2F_1\left(1/2 - \nu, 1/2; 1; \frac{A'' - C''}{A''}\right) \tag{34}$$

In a highly anisotropic medium ($a \gg 1$ and $b = 1$) with propagation angles well removed from the direction of the principal axis, $A'' \sim a^2$ and $C'' \sim 1$. Moreover, $\lim_{z \to 1} {}_2F_1(1/2 - \nu, 1/2; 1; z) = \Gamma(\nu)/[\sqrt{\pi}\,\Gamma(\nu + 1/2)]$, which is also the limiting value of $\mathscr{J}$ as $a \to \infty$. It can be shown by direct computation that this limit gives the correct form of S_4 when a strictly two-dimensional irregularity model is used.

Equation (31) admits a simple and intuitive interpretation. Recall that for a three-dimensional SDF of the form $C_s q^{-(2\nu+1)}$ the corresponding one-dimensional SDF obtained by integrating over two of the three spatial variables is proportional to $C_s q^{-(2\nu-1)}$. Thus if the three-dimensional SDF varies as q^{-4}, then the one-dimensional SDF will vary as q^{-2}. Since $S_4^2 \propto C_s (1/\sqrt{Z})^{-(2\nu-1)}$, it follows that the magnitude of S_4 is 'driven' by the intensity of the one-dimensional irregularity SDF evaluated at the spatial wave number corresponding to the Fresnel radius. This is an intuitively satisfying result, but it can be confusing vis a vis the early scintillation theory based on a gaussian ACF. There is, for example, no region of far-zone behavior. Moreover, the rms phase level cannot be uniquely related to S_4.

4. APPLICATION TO DATA ANALYSIS

The theoretical development presented in sections 2 and 3 was motivated by preliminary analyses of scintillation data from the Wideband satellite which transmits phase coherent signals at S band, L band, UHF, and VHF. By using the S-band signal as a phase reference, intensity and phase scintillation measurements can be made at all the lower frequencies.

As is described in the work of *Fremouw et al.* [1978], a high-pass filter with a sharp cutoff at 0.1 Hz is used to separate the slow phase trends from the phase scintillation in the routine data processing. The detrended data are then processed in 20-s segments, and phase SDF's are computed at UHF and VHF. The measured phase SDF's are then smoothed and fitted (using log-linear least

squares) to the analytic form Tf^{-p}. The parameters T and p can then be interpreted by using the theory developed in section 2.

The theory developed in section 2, however, neglects diffraction effects in the phase scintillation data. Nonetheless, it was noted very early from the Wideband data that the wavelength dependence of the rms phase is very accurately predicted by (1) [*Fremouw et al.*, 1978]. This fact alone does not prove that T and p are unaffected by diffraction, but to the extent that the model is correct, p should be independent of wavelength, whereas T should scale with frequency as $\lambda^2(1 - f^2/f_r^2)^2$.

Let us first consider the power law index p. In Figures 1*a* and 1*b*, measured values of p at VHF and UHF are plotted against the corresponding S_4 values for a large sample of data passes that were recorded at the Wideband equatorial tracking stations at Ancon, Peru, and at Kwajalein in the Marshall Islands. For small S_4 values, noise contamination causes low measured p values. For large S_4 values, the rapid phase changes associated with the frequently occurring deep fades should drive the measured phase SDF toward f^{-2}, which is the high-frequency asymptote of the power spectrum of any discontinuous random process. The error bars denote the measured standard deviation of the data. These results show that for comparable S_4 levels, p is independent of frequency.

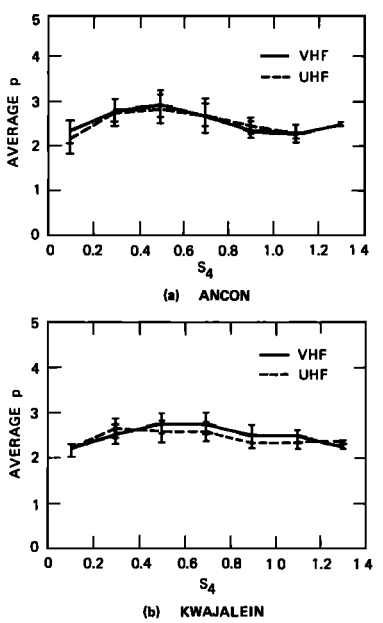

Fig. 1. Average value of p versus S_4 values within the intervals $0.2n \leq S_4 \leq 0.2(n + 1)$ for equatorial data.

In the S_4 range where both noise contamination and strong scatter effects are evidently negligible, however, the measured p values are lower than the nominal value ($p = 3$) that is usually reported [*Crane*, 1977]. Moreover, there is a systematic difference between the Kwajalein and Ancon data, the latter station showing somewhat steeper slopes. The self-consistency of the phase and amplitude data against the theory substantiates the measured slopes.

To verify this, (20) is first applied to calculate σ_ϕ using the measured T values and a fixed value of $\nu(p = 2\nu)$ with $\tau_c = 10$ s. A fixed value is used rather than the measured value to avoid confusion due to the S_4 dependence of p shown in Figure 1. From the known satellite position and velocity, and an assumed equivalent phase-screen height and irregularity anisotropy, (18) can then be used to compute (L sec θ) C_s. Finally, (31) is used to calculate S_4 for comparison with the measured value.

The results of applying this procedure to UHF data from a moderately disturbed Ancon pass is shown in Figure 2. In the weakly disturbed portion of the pass (~0338:30 to ~0344:15), the $\nu = 1.3$ ($p = 2.6$) theoretical curve for σ_ϕ fits the measured rms phase somewhat better than the $\nu = 1.5$ curve. Moreover, S_4 calculations for an equivalent phase screen located in the F region (350 km) with $\nu = 1.3$ fit the data better than the corresponding calculations for $\nu = 1.5$. Thus the general behavior of S_4 is consistent with the separately measured p values less than 3, although the model calculations consistently overestimate the measured S_4 values.

To explain this effect, consider the altitude dependence of S_4. In the routine summary analysis of the Wideband data the propagation geometry is computed only for two reference altitudes, namely, 110 km (E region) and 350 km (F region). Thus the reference altitude is not varied continuously. Nonetheless, it is clear from the general trend of decreasing S_4 with increasing altitude, that a better fit to the data would be obtained for an altitude higher than 350 km.

The reason S_4 decreases with increasing altitude comes from the conversion of T to C_s (see (18)). The effective scan velocity v_{eff} increases with increasing altitude. Thus for a given T level the corresponding C_s value, which drives the S_4 level, is much smaller (v_{eff} enters (18) raised to the 2ν

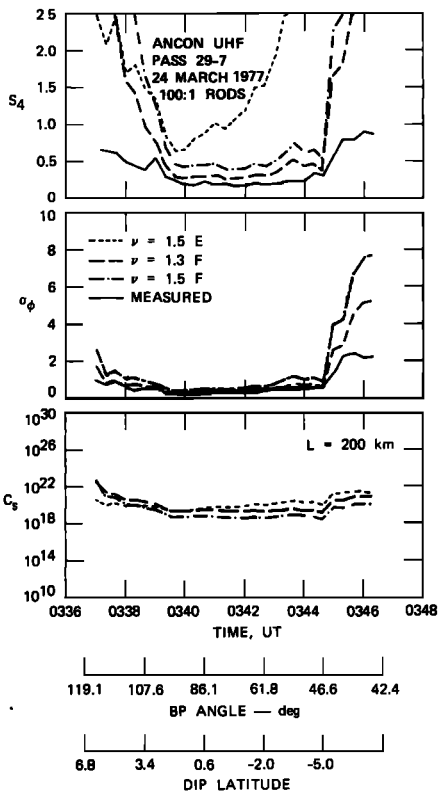

Fig. 2. Data from Ancon pass 29-7 together with theoretical curves showing the effects of changing effective layer height and spectral slopes. (The BP (Briggs-Parkin) angle is the angle between the propagation vector and the local magnetic field direction at 350 km.)

− 1 power) than the corresponding value for lower altitudes. This effect completely dominates the opposite altitude dependence of S_4 imposed by the height dependence of Z.

The model is very sensitive to small changes in the spectral index ν and the layer height. However, the equatorial calculations are insensitive to the actual value of the axial ratio as long as a $\geq$ 10. Under strong scatter conditions the model overestimates S_4, since extinction is not accounted for. Moreover, it has already been noted that the phase SDF tends toward f^{-2} under strong scatter conditions, which explains the discrepancies between the measured rms phase and the model computations for fixed ν.

In the bottom panel of Figure 2 the C_s values that correspond to a 200-km-thick scattering layer are shown to give some idea of the order of magnitude of the C_s values associated with various S_4 levels. The actual value of C_s depends on the length unit which was taken to be meters.

In Figures 3 and 4, two additional Ancon examples are shown. In Figure 3 the S_4 values are generally small, and the theory works very well. In Figure 4, conditions are more disturbed, and the model consistently overestimates S_4. Nonetheless, with the exception of the initial few minutes of the pass where $S_4 \sim 1.0$, the rms phase measurements are accurately reproduced. Thus the C_s estimates are accurate even for large S_4 values. Of course the effective phase screen height must also be determined.

The data from Kwajalein show very similar results. Self-consistent modeling of the phase spectrum and the measured scintillation index S_4 can be obtained for effective layer heights at 350 km or above and spectral slopes somewhat smaller (flatter SDF's) than the Ancon data. In section 5 the applicability of these results to the gigahertz scintillation phenomenon is discussed.

Wideband satellite data have also been recorded at Poker Flat, Alaska, which is in the auroral zone.

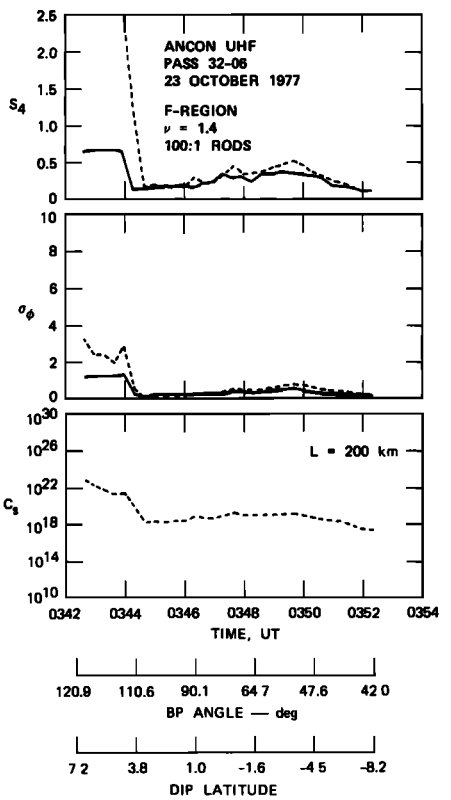

Fig. 3. Data from Ancon pass 32-06 together with theoretical curves showing good fits under weak scatter conditions.

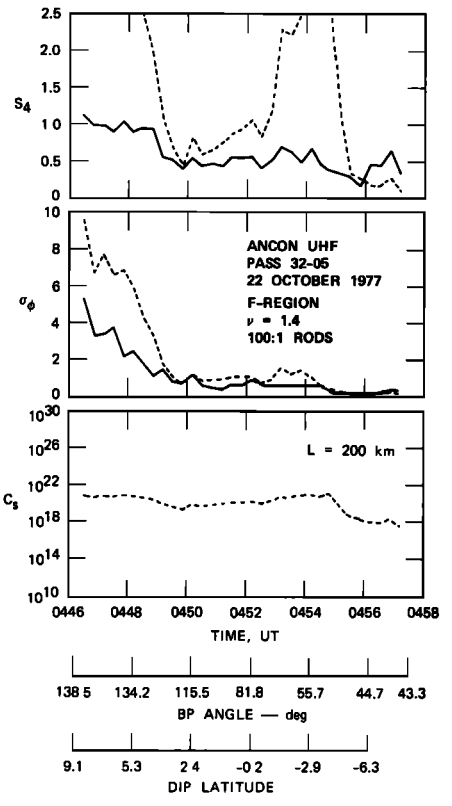

Fig. 4. Data from Ancon pass 32-05 together with theoretical curves derived with the same parameters as were used in Figure 3.

The high-latitude scintillation data are complicated by the rapidly changing propagation geometry, the pronounced latitudinal variation of auroral phenomena, and local inhomogeneities such as discrete auroral arcs. Nonetheless, the model calculations have produced consistent results where well-developed scintillation is present.

In Figure 5, p versus S_4 curves are shown for the auroral data. The p values are considerably smaller than 3. *Phelps and Sagalyn* [1976] report an in situ power law index of 1.6, which implies a somewhat larger value for p than the Wideband data are showing. Also, because intense UHF scintillation in the auroral zone is both infrequent and highly localized when it does occur, the UHF curve does not extend beyond $S_4 \cong 0.7$.

Now, as is shown by *Rino et al.* [1978], there is a high probability of enhanced auroral zone phase and amplitude scintillation where the propagation path intercepts the local L shell. Thus as a first detailed example of auroral zone scintillation, Figure 6 exhibits data from a pass showing an isolated scintillation enhancement. Because of the near meridional geometry of the pass, the point of L-shell coincidence is also the point where the Briggs-Parkin angle achieves its minimum value.

The localized scintillation enhancement can be explained if the auroral irregularities have a sheet-like anisotropy. That is, the irregularities have a high degree of coherence both along and across the magnetic field in the direction of the local L shell. Thus in the model computations the parame-

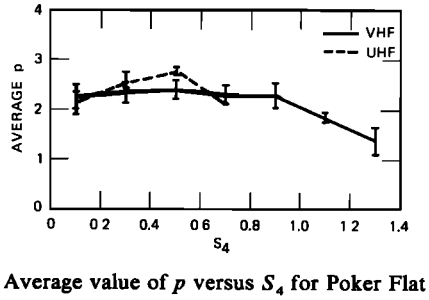

Fig. 5. Average value of p versus S_4 for Poker Flat data.

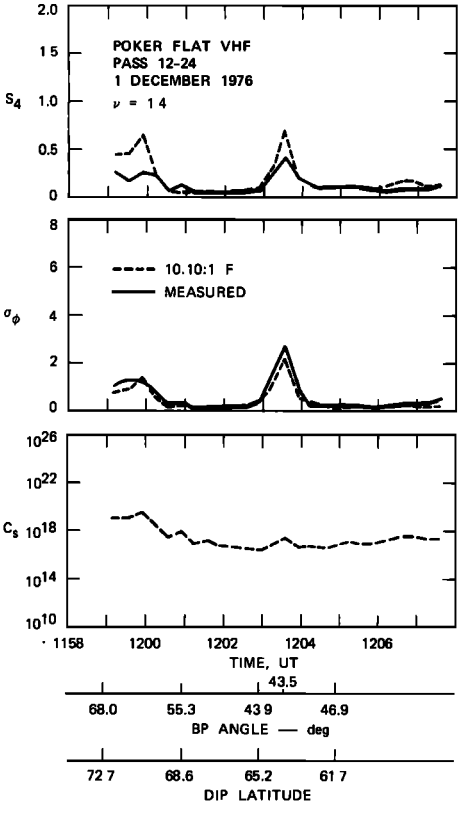

Fig. 6. Data from Poker Flat pass 12-24 showing isolated geometrical enhancement attributed to sheetlike irregularities.

ters $a = 10$, $b = 10$, and $\delta = 0$ are used.

There is distortion of the phase SDF in the region of the geometrical enhancement which is attributed to the rapid change in the propagation geometry. In Figure 6 the overshoot of the calculated S_4 value at the geometrical enhancement is due to the spectral distortion as well as the elevated scintillation level.

In Figure 7 an example of more disturbed auroral scintillation is shown. The phase scintillation data fit the model computations using $\nu = 1.25$ better than with $\nu = 1.5$. Also, by comparing the intensity scintillation from 0907 to 0909 UT and from 0909 to 0911 UT a change in altitude from the E region to the F region can be inferred.

The examples presented in this section show that the power law phase screen model can be used to self-consistently reproduce measured phase and intensity scintillation under conditions of weak scattering ($S_4 \leq 0.4$). The geometrical dependence of the scattering under very different propagation geometries is easily accommodated. Finally, for a specified effective layer thickness a geometry-independent strength of turbulence parameter can be derived.

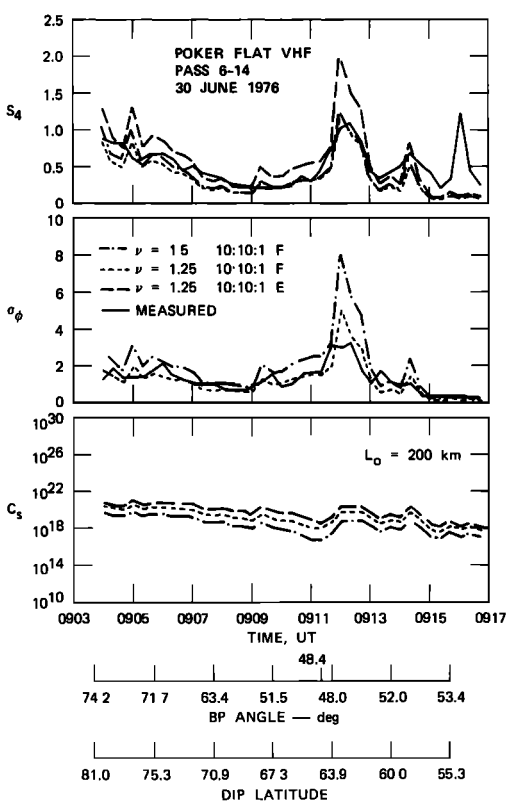

Fig. 7. Data from Poker Flat pass 6-14 together with theoretical curves showing evidence of height change.

5. DISCUSSION

It has been shown that a comparatively simple model can be used to interpret ionospheric amplitude and phase scintillation data under conditions of weak scatter. Formally, the disturbed region is replaced by an equivalent phase changing screen. The model fully accounts for the angle dependence of σ_ϕ and S_4 in a three-dimensional anisotropic medium. Moreover, the formulas converge to forms that can be obtained directly from a two-dimensional model as the axial ratio approaches infinity.

The model computations are based on a power law irregularity SDF. The power law index is variable, and the effects of an arbitrarily large outer scale are explicitly revealed in the model computations. The data analysis shows that the spectral index p is variable but generally less than 3, and there is no evidence of a finite outer-scale cutoff within data intervals that can be considered to be statistically homogeneous.

The major limitation of the model, which is fundamental to any scintillation measurement, is that the scintillation structure is the integrated effect of all irregularities along the propagation path. Aside from assigning all the diffraction to free space, which is not a serious defect [*Bramley*, 1977], the phase screen model assumes a uniform propagation geometry and irregularity structure along the propagation path.

In reality, both the propagation angles relative to magnetic field and the irregularity structure vary along the propagation path. However, the fact that the equivalent parameters deduced from the phase screen model self-consistently reproduce the amplitude and phase scintillation levels verifies the validity of the model for predicting scintillation effects. The detailed relation of the equivalent parameters to the in situ structure remains to be demonstrated.

It is instructive to consider the simplest possible case. The three-dimensional ACF corresponding to (6) is

$$R_{\Delta N_e}(y) = \frac{C_s}{4\pi^{3/2}\Gamma(\nu + 1/2)} \left| \frac{y}{2q_0} \right|^{\nu-1} K_{\nu-1}(q_0 y) \tag{35}$$

which is similar to (12). The corresponding one-dimensional temporal SDF, which would be mea-

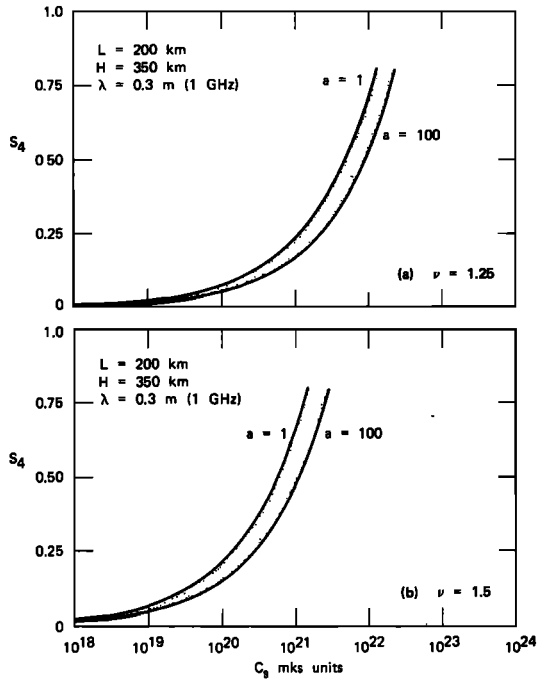

Fig. 8. Calculated scintillation at 1 GHz for idealized equatorial geometry.

sured by an in situ electron density probe, is

$$\varphi_P(f) = \frac{C_s \Gamma(\nu - 1/2)}{4\pi^2 \Gamma(\nu + 1/2)} \frac{1}{v_p (q_0^2 + (2\pi f / v_p)^2)^{\nu - 1/2}} \tag{36}$$

where v_p is the effective probe velocity which is a quadratic form in the x, y, and z components of the true probe velocity ($v_p^2 = \vec{v}^T \mathbf{C} \vec{v}$, where $\vec{v}$ is the probe velocity and the matrix $\mathbf{C}$ is defined in section 4 of *Rino and Fremouw* [1977]).

As with the phase SDF, when $2\pi f / v_p \gg q_0$, $\varphi_p(f) = T_p f^{-(2\nu - 1)}$, where

$$T_p = \frac{C_s \Gamma(\nu - 1/2)}{4\pi^2 \Gamma(\nu + 1/2)} \frac{1}{v_p (2\pi / v_p)^{2\nu - 1}} \tag{37}$$

Thus if the probe velocity relative to the magnetic field is known, (37) can be used to deduce C_s in terms of the measured in situ spectral index and turbulent strength C_s.

In Figure 8, (31) has been evaluated for propagation normal to the magnetic field at 1 GHz. It can be seen that C_s values greater than 10^{21} will produce significant gigahertz scintillation levels if the irregularities are distributed uniformly over a 200-km path. Since such phenomena are known to occur near the geomagnetic equator, an in situ probe such as the AE-E satellite [*McClure et al.*, 1977] should measure consistent T_p values if the model is valid.

The measured rms electron density can be estimated by using (20) with T replaced by T_p and p replaced by $2\nu - 1$. The time interval τ_c is the duration of the data segment used to measure the in situ SDF.

Acknowledgment. This work was supported by the Defense Nuclear Agency under contract DNA001-77-C-0220.

REFERENCES

Booker, H. G., and J. A. Ferguson (1978), A theoretical model for equatorial ionospheric spread *F* echoes in the HF and VHF bands, *J. Atmos. Terr. Phys., 40,* 803.

Booker, H. G., J. A. Ratcliffe, and D. H. Shinn (1950), Diffraction from an irregular screen with applications to ionospheric problems, *Phil. Trans. Roy. Soc. Ser. A., 242,* 579.

Bramley, E. N. (1954), The diffraction of waves by an irregular refracting medium, *Proc. Roy. Soc. Ser. A., 225,* 515.

Bramley, E. N. (1977), The accuracy of computing ionospheric radio-wave scintillation by the thin-phase-screen approximation, *J. Atmos. Terr. Phys., 39,* 367.

Briggs, B. H., and I. A. Parkin (1963), On the variation of radio star and satellite scintillations with zenith angle, *J. Atmos. Terr. Phys., 25,* 339.

Costa, E., and M. C. Kelley (1976), Calculations of equatorial scintillations at VHF and gigahertz frequencies based on a new model of the disturbed equatorial ionosphere, *Geophys. Res. Lett., 3,* 677.

Crane, R. (1976), Spectra of ionospheric scintillation, *J. Geophys. Res., 81,* 2041.

Crane, R. (1977), Ionospheric scintillation, *Proc. IEEE, 65,* 180.

Dyson, P. L., J. P. McClure, and W. B. Hanson (1974), In situ measurements of the spectral characteristics of *F*-region ionospheric irregularities, *J. Geophys. Res., 79,* 1497.

Fremouw, E. J., R. L. Leadabrand, R. C. Livingston, M. D. Cousins, C. L. Rino, B. C. Fair, and R. A. Long (1978), Early results from the DNA Wideband satellite experiment—Complex-signal scintillation, *Radio Sci., 13,* 167.

Gradshteyn, I. S., and I. M. Ryzhik (1965), *Table of Integrals Series and Products,* Academic, New York.

McClure, J. P., W. B. Hanson, and J. H. Hoffman (1977), Plasma bubbles and irregularities in the equatorial ionosphere, *J. Geophys. Res., 82,* 578.

Mercier, R. P. (1962), Diffraction by a screen causing large random phase fluctuations, *Proc. Cambridge Phil. Soc., 58,* 382.

Phelps, A. D. R., and R. C. Sagalyn (1976), Plasma density irregularities in the high-latitude topside ionosphere, *J. Geophys. Res., 81,* 515.

Ratcliffe, J. A. (1956), Some aspects of diffraction theory and their application to the ionosphere, *Rep. Phys. Soc. Progr. Phys., 19,* 188.

Rino, C. L., and E. J. Fremouw (1977), The angle dependence of singly scattered wavefields, *J. Atmos. Terr. Phys., 39,* 859.

Rino, C. L., R. C. Livingston, and S. J. Matthews (1978), Evidence for sheet-like auroral ionospheric irregularities, *Geophys. Res. Lett., 5,* 1039.

Rufenach, C. L. (1972), Power-law wave number spectrum deduced from ionospheric scintillation observations, *J. Geophys. Res., 77,* 4761.

Rufenach, C. L. (1975), Ionospheric scintillation by a random phase screen: Spectral approach, *Radio Sci., 10,* 155.

Rumsey, V. H. (1975), Scintillations due to a concentrated layer with a power law turbulence spectrum, *Radio Sci., 10,* 107.

Salpeter, E. E. (1976), Interplanetary scintillations, I, Theory, *Astrophys. J., 147,* 433.

Strohbehn, J. W. (1968), Line-of-sight wave propagation through the turbulent atmosphere, *Proc. IEEE, 56,* 1301.

Yeh, K. C., and C. H. Liu (1977), Diagnosis of the turbulent state of ionospheric plasma by propagation methods, *Radio Sci., 12,* 1031.